

Preparation and photocatalytic performance of Sn-doped and BiOI-coupled dual modified Bi₂WO₆ composite

Q. Qin^a, L. Zhang^b, T. Xiao^b, Y. Y. Zhong^b, J. Wang^{b, c}, W. L. Liang^a, Y. H. Wang^a, S. C. Yang^a, X. D. Zhu^{b, *}

^a*Intelligent Manufacturing College, Chengdu Jincheng College, Chengdu 611731, China*

^b*School of Mechanical Engineering, Chengdu University, Chengdu, 610106, China*

^c*Sichuan Institute of Industrial Technology, Deyang, 618000, China*

Sn doped and BiOI coupled dual modified Bi₂WO₆ photocatalytic material was prepared using hydrothermal route. The phase composition, morphology, surface area, elemental composition and oxidation state, as well as optical properties, were comprehensively characterized. Take the methylene blue (MB) as the model pollutant for photodegradation to estimate the photocatalytic property of the synthesized material. The prepared Bi₂WO₆-based composite material shows a flower-like structure assembled from nanosheets, with a surface area of 45.3 m²/g and a bandgap width of 2.41 eV, enabling visible light responsiveness. The synergistic effect of Sn doping and BiOI coupling modification enhances the photocatalytic performance. The Sn-BiOI/Bi₂WO₆ photocatalytic composite material shows excellent photocatalytic activity, with complete degradation of MB after 40 minutes of illumination, and a first-order reaction rate constant (k) of 0.102 min⁻¹. Experimental evidence suggests that photoinduced holes are the main active species.

(Received January 25, 2024; Accepted April 9, 2024)

Keywords: Bi₂WO₆, Sn doping, BiOI coupling, Photocatalytic activity

1. Introduction

Utilizing photocatalysts to degrade pollutants under light irradiation is an effective method for treating water pollution [1-3]. In recent years, there has been widespread attention on photocatalytic materials that respond to visible light to increase solar light utilization. Bi₂WO₆, due to its unique layered structure, appropriate bandgap width, and relatively large specific surface area, has become a focal point in the research of photocatalytic materials [4-6]. The pure Bi₂WO₆ exhibits easy reunion of photoinduced charge, and its quantum efficiency needs improvement [7, 8]. Therefore, a series of modifications are required to enhance quantum utilization and improve photocatalytic performance. Common modification strategies include ion doping and semiconductor coupling [9-15]. Zhang et al [10]. modified Bi₂WO₆ through Γ doping and found that the modified material exhibited reduced charge transfer resistance, increased separation of photoinduced electrons and holes, and a significantly enhanced removal rate of Hg ions. Cheng et al [12]. prepared Bi₂WO₆/ZnO composite materials, forming a type II semiconductor structure. At the interface, photoinduced electrons moved from the Bi₂WO₆ conduction band (CB) to the ZnO CB, while holes migrated from the ZnO valence band (VB) to the Bi₂WO₆ VB, which increased the charge separation efficiency, demonstrating higher photocatalytic activity compared to pure Bi₂WO₆.

In the previous work, modifications were separately applied to pure Bi₂WO₆ through Sn doping and BiOI coupling, and the results indicated that both methods could enhance photocatalytic activity [16-18]. Combining different modification methods allows the exploitation of the respective advantages of each method, creating a synergistic effect to further improve photocatalytic performance on the basis of a single modification method. Therefore, in this work, hydrothermal route was employed to synthesis a dual modified Bi₂WO₆ photocatalyst with Sn

* Corresponding author: xiaodangjia21@126.com
<https://doi.org/10.15251/DJNB.2024.192.549>

doping and BiOI coupling (Sn-BiOI/Bi₂WO₆). The microstructure of the catalyst was extensively investigated through techniques like scanning electron microscopy (SEM), transmission electron microscopy (TEM), X-ray photoelectron spectroscopy (XPS), surface area analysis (BET), X-ray diffraction (XRD), ultraviolet-visible absorption spectrum (DRS), and photoluminescence spectrum (PL). Taking MB as the target pollutant for photodegradation to estimate the photocatalytic property, and the active species during the photodegradation process were analyzed simultaneously.

2. Experimental

2.1. Synthesis of photocatalytic material

Bi(NO₃)₃·5H₂O and CH₃COOH were put in 20 mL purified water, and a certain amount of sodium iodide and stannous chloride were added to form solution A, with a Sn/Bi atomic ratio of 2% and an I/W atomic ratio of 40%. Na₂WO₄·2H₂O was mixed with 12 mL purified water to form solution B, with a mass ratio of Bi(NO₃)₃·5H₂O to Na₂WO₄·2H₂O of 2.94:1. Put Solution B in solution A with continuous agitating for 30 min until flocculent forms. The obtained suspension was shifted to a container and subjected to a hydrothermal treatment at 160 °C for 24 hours. The product was cleaned by purified water and anhydrous ethanol till neutral, dried, and then ground to obtain Sn-BiOI/Bi₂WO₆ powder.

2.2. Characterization technology

XRD was employed to analyze the phase composition, SEM, TEM, and BET were adopted to study the morphology and specific surface area, EDS and XPS were employed to clarify the element composition and chemical state, and DRS and PL spectroscopy were used to study its optical properties.

2.3. Photocatalytic experiment

25 mg Sn-BiOI/Bi₂WO₆ powder was mixed to 100 mL MB aqueous solution (10 mg/L) and agitated. After dark adsorption for 30 minutes, the xenon lamp light source (250 W, 300-800 nm) was turned on for the reaction. The mixture was taken every 10 minutes, and the upper clear solution was separated after centrifugation. The absorbance (664 nm) was measured, and the degradation degree was determined by the formula $(A_0 - A_t)/A_0$, where A_0 and A_t are the primary absorbance of MB and the absorbance at time t , respectively.

Add isopropanol (IPA) to capture ·OH, benzoquinone (BQ) to seize ·O₂⁻, and ammonium oxalate (AO) to seize photogenerated holes (h⁺). Compare with blank experiments and analyze the active groups in the photocatalytic process [19, 20]. Specifically, 2 mL (2 mmol/L) IPA, BQ and AO solutions were put into the photocatalytic reaction system during the experiment, and the degradation degrees after adding scavengers were calculated by comparing with the blank experiment result.

3. Results and discussion

3.1. Phase composition

Figure 1 gives the XRD pattern of Sn-BiOI/Bi₂WO₆. The diffraction peaks around 28.3°, 32.9° and 47.2° ascribe to the Bi₂WO₆ (131), (200) and (202) planes, Additionally, diffraction peaks at 29.6°, 31.7° and 39.4° correspond to the BiOI (102), (110) and (004) planes, indicating the formation of BiOI/Bi₂WO₆ composite material. No diffraction peaks related to Sn were detected, possibly as the ionic radius of Sn⁴⁺ (0.069 nm) is smaller than Bi³⁺ (0.103 nm), allowing Sn⁴⁺ to enter the Bi₂WO₆ lattice without reacting to form new phases [21].

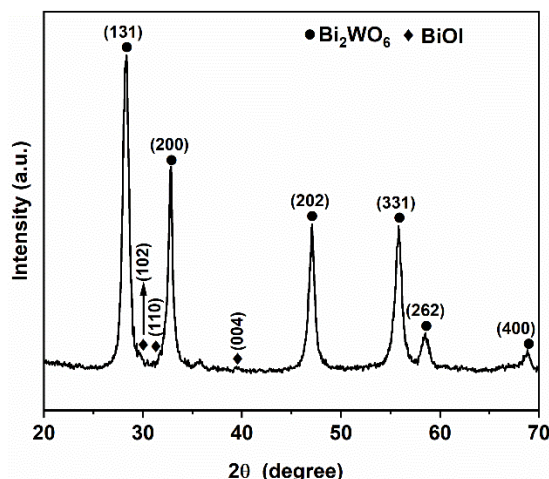


Fig. 1. XRD pattern of Sn-BiOI/Bi₂WO₆.

3.2. Morphology and specific surface area analysis

Figure 2 displays the SEM images of Sn-BiOI/Bi₂WO₆. The prepared Sn-BiOI/Bi₂WO₆ shows a flower-like structure assembled from nanosheets. This structure is beneficial for rising the surface area, affording more reaction sites and enhancing the adsorption of pollutant molecules [22].

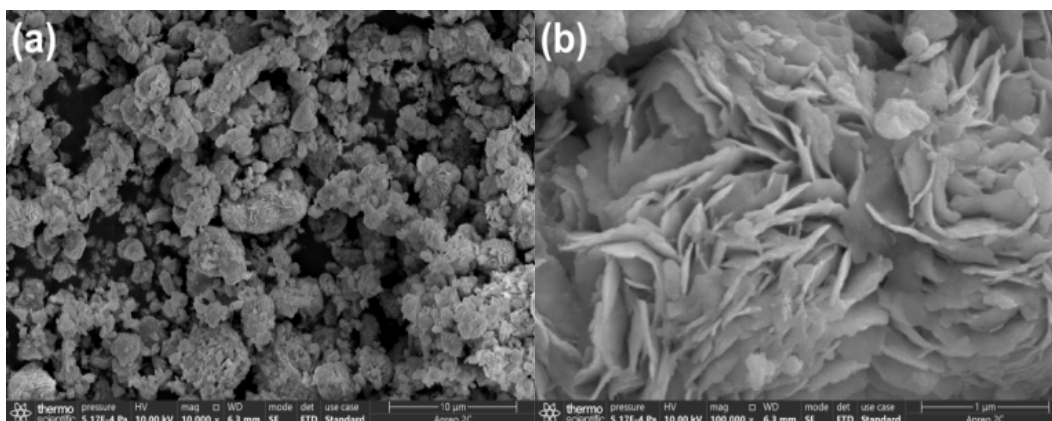


Fig. 2. SEM images of Sn-BiOI/Bi₂WO₆.

Figure 3 shows the EDS mappings of Sn-BiOI/Bi₂WO₆, revealing the presence of five elements: Bi, W, O, I, and Sn, distributed uniformly throughout the sample.

Figure 4 presents the TEM (a, b, c) and HRTEM (d) images of Sn-BiOI/Bi₂WO₆, indicating that the three-dimensional flower assembled from two-dimensional nanosheets has a diameter of approximately 1 μm. The labeled crystal plane distances of 0.318 nm and 0.302 nm (Figure 4d) correspond to the Bi₂WO₆ (131) and the BiOI (102) planes [10, 12], evidencing the formation of BiOI/Bi₂WO₆ composite material, in accordance with the XRD results.

Figure 5 (a) is the pore size distribution curve. The pore sizes are distributed mainly between 2 nm and 10 nm. Figure 5 (b) is N₂ adsorption-desorption isotherm of Sn-BiOI/Bi₂WO₆, and the surface area is determined to be 45.3 m²/g. Previous research showed that the specific surface areas of pure Bi₂WO₆, Sn-doped Bi₂WO₆ and BiOI/Bi₂WO₆ were 20.8 m²/g, 41.8 m²/g and 27.9 m²/g [16-18]. This indicates that both Sn doping and BiOI coupling contribute to the increased surface area, and the combination of these two modifications further enhances the specific surface area.

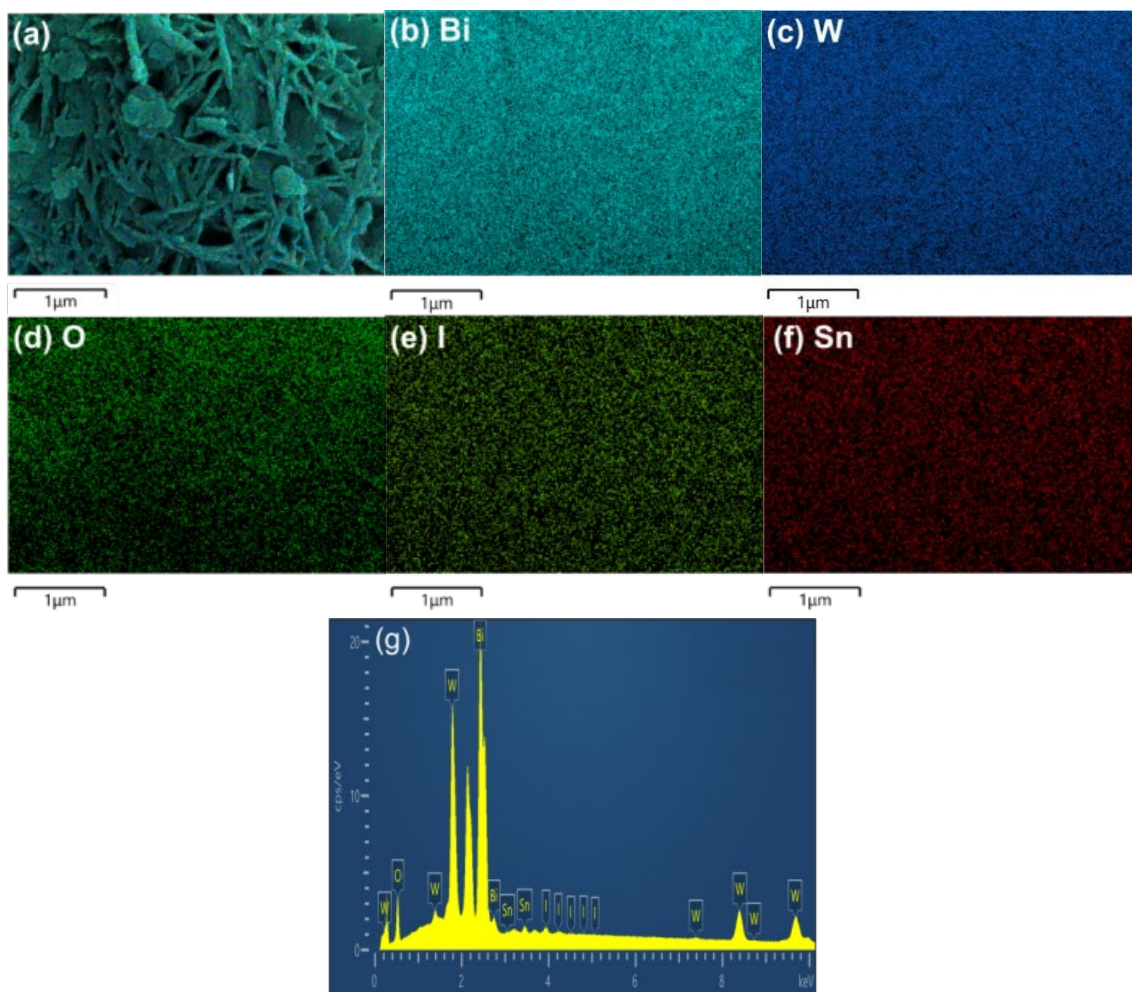


Fig. 3. EDS mappings of Sn-BiOI/Bi₂WO₆.

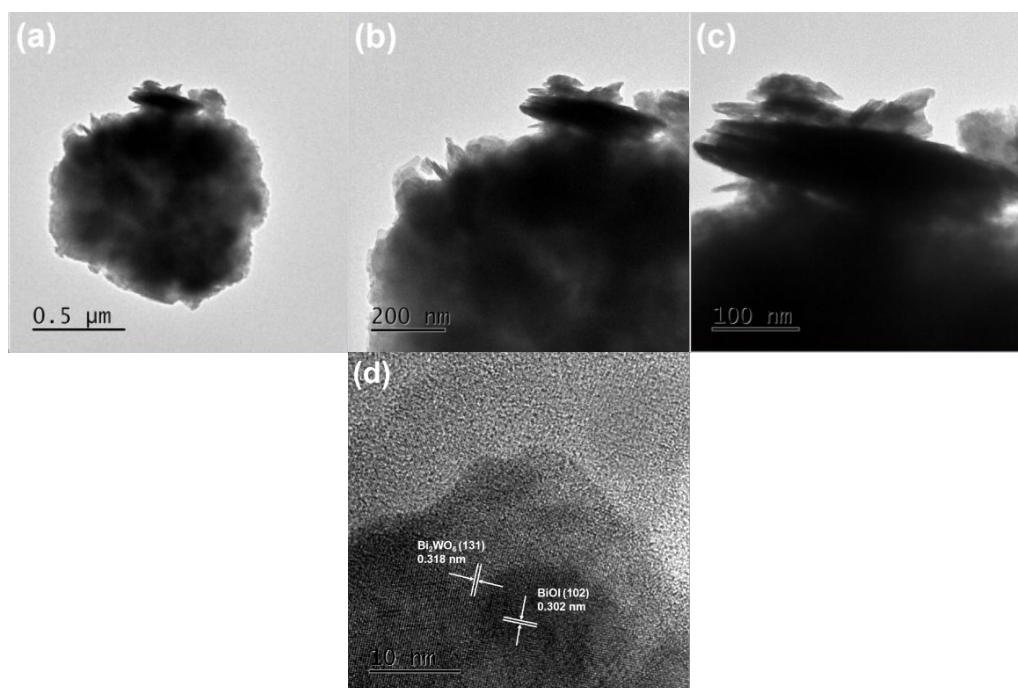


Fig. 4. TEM and HRTEM images of Sn-BiOI/Bi₂WO₆.

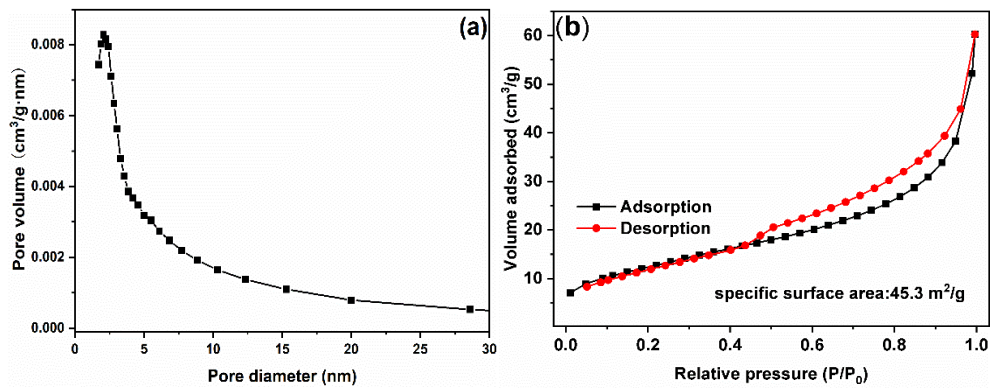


Fig. 5. Pore size distribution curve (a) and N_2 adsorption-desorption isotherm (b) of $Sn-BiOI/Bi_2WO_6$.

3.3. Elemental chemical state analysis

Figure 6 gives the XPS spectra of $Sn-BiOI/Bi_2WO_6$. In figure 6 (a), the overall spectrum reveals peaks corresponding to the signals of the five elements Bi, W, O, Sn, and I, which is in accordance with the EDS mappings.

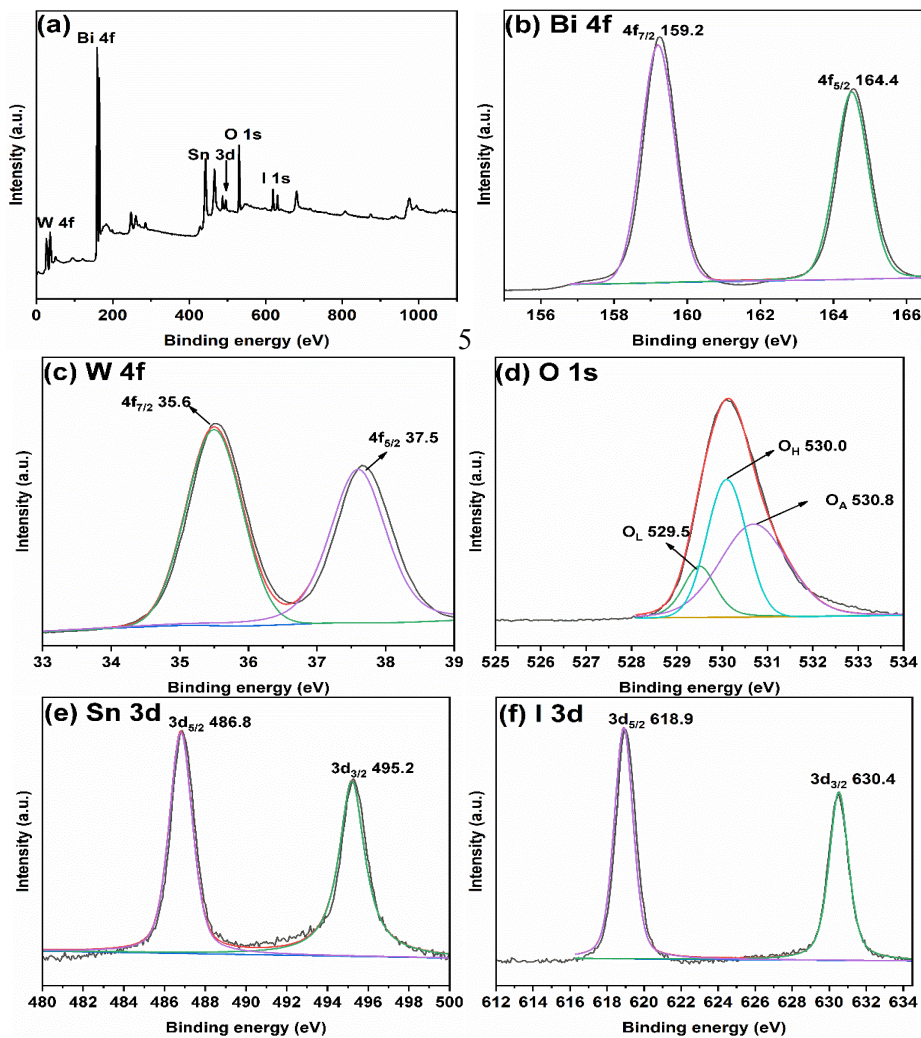


Fig. 6. XPS spectrum of $Sn-BiOI/Bi_2WO_6$: (a) total spectrum; (b) Bi 4f; (c) W 4f; (d) O 1s; (e) Sn 3d and (f) I 3d.

Figure 6 (b) displays the spectrum of Bi 4f, showing two peaks situated at 159.2 eV and 164.4 eV, ascribing to Bi 4f_{7/2} and Bi 4f_{5/2}, indicating that the Bi element is +3 state [13, 23]. In Figure 6 (c), the peaks around 37.5 eV and 35.6 eV correspond to W 4f_{5/2} and W 4f_{7/2}, confirming that W is +6 state [13, 23]. The O 1s peak can be decomposed into lattice oxygen, surface hydroxyl groups and absorbed oxygen, situated at 529.5 eV, 530.0 eV and 530.8 eV [15, 20]. The peaks around 486.8 eV (Sn 3d_{5/2}) and 495.2 eV (Sn 3d_{3/2}) implies the presence of Sn⁴⁺ [23]. I 3d peaks are located at 630.4 eV (I 3d_{3/2}) and 618.9 eV (I 3d_{5/2}), suggesting that the chemical oxidation state of I is -1 [24].

3.4. Optical property analysis

Figure 7 displays the ultraviolet-visible absorption spectrum of Sn-BiOI/Bi₂WO₆, showing an absorption edge located around 500 nm. The bandgap width (E_g) was determined by the formula $\alpha h\nu = A(h\nu - E_g)^{1/n}$, n is related to the semiconductor type (n = 1/2 for direct semiconductor and n = 2 for indirect semiconductor). The calculated bandgap width of Sn-BiOI/Bi₂WO₆ is determined to be 2.41 eV, indicating visible light responsiveness.

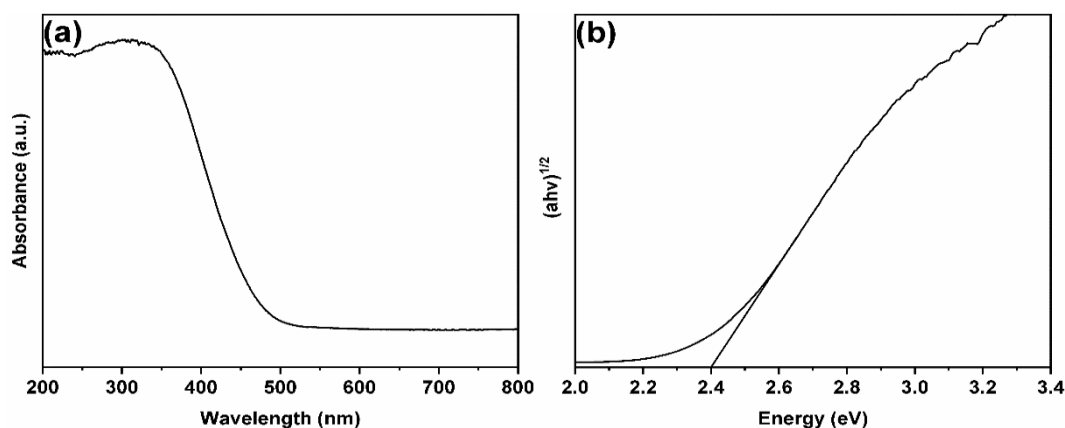


Fig. 7. Ultraviolet-visible absorption spectrum (a) and band gap (b) of Sn-BiOI/Bi₂WO₆.

Figure 8 presents the photoluminescence spectrum (PL) of Sn-BiOI/Bi₂WO₆, and compares with the PL spectrum of pure Bi₂WO₆ [16], its intensity is significantly reduced. This decrease in intensity suggests a significant reduction in the recombination degree of photogenerated charges in the composite material, leading to an improvement in quantum efficiency.

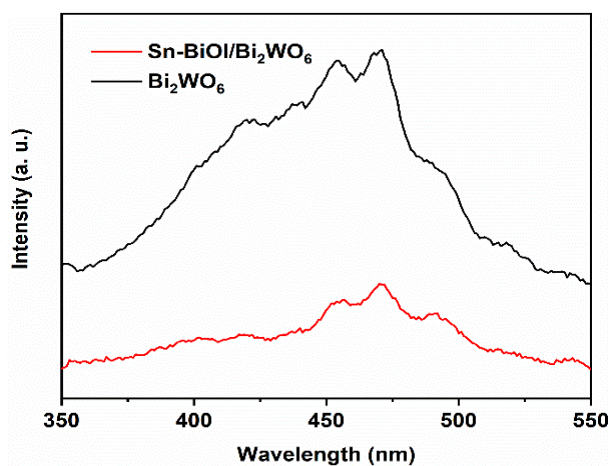


Fig. 8. PL spectra of pure Bi₂WO₆ and Sn-BiOI/Bi₂WO₆.

3.5. Photocatalytic activity and photocatalytic mechanism

Previous researches results indicated that both Sn doping and BiOI coupling modification could enhance the photocatalytic activity of Bi_2WO_6 . The k for pure Bi_2WO_6 , Sn-doped Bi_2WO_6 , and $\text{BiOI}/\text{Bi}_2\text{WO}_6$ were 0.015 min^{-1} , 0.030 min^{-1} , and 0.089 min^{-1} [16-18]. Figure 9 shows the MB photodegradation curve (a) and the kinetics fitting curve (b) of Sn-BiOI/ Bi_2WO_6 . The results indicate complete degradation of MB after 40 minutes of illumination, with k of 0.102 min^{-1} . This suggests that the photocatalytic performance of the dual modified Bi_2WO_6 not only surpasses that of pure Bi_2WO_6 but also outperforms the photocatalytic performance of samples modified with a single method. Figure 10 presents the experimental results of active species. AO adding significantly reduces the discoloration degree, revealing that h^+ are the main active species.

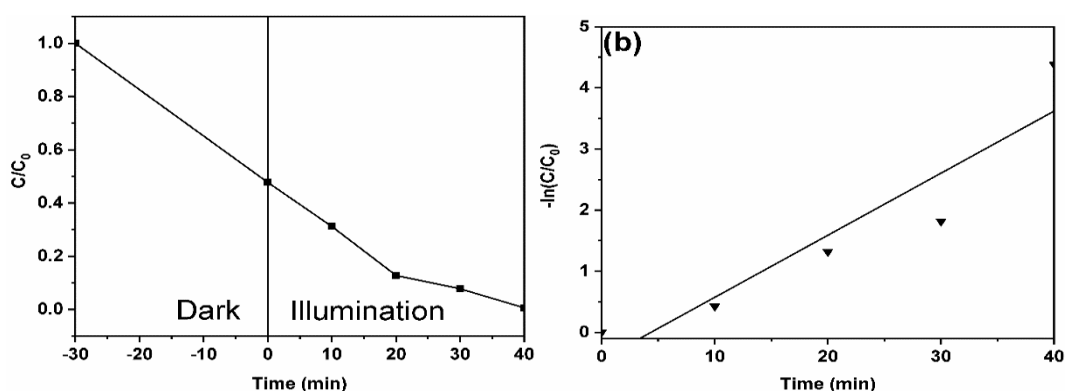


Fig. 9. Photocatalytic degradation curve of MB (a) and kinetics fitting curve (b) of Sn-BiOI/ Bi_2WO_6 .

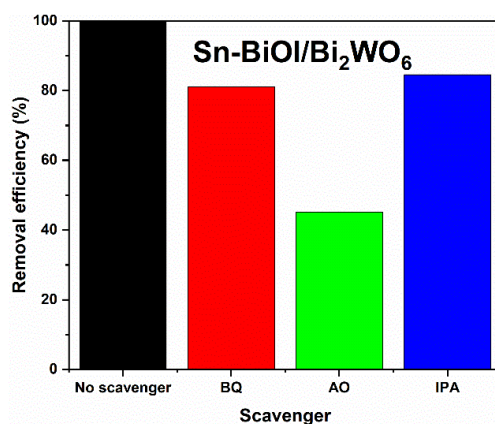


Fig. 10. Active species capture experiment of Sn-BiOI/ Bi_2WO_6 .

The photodegradation results demonstrate that the synergistic effect of Sn doping and BiOI coupling modification enhances the photocatalytic performance of Bi_2WO_6 . The photoinduced charge transfer mechanism in Sn-BiOI/ Bi_2WO_6 is proposed in Figure 11. On one hand, after Sn doping, Sn^{4+} may enter the interior of Bi_2WO_6 lattice, causing lattice defects that can capture photogenerated charges and improve charge separation efficiency [25]. On the other hand, the coupling of BiOI with Bi_2WO_6 forms a semiconductor junction. Due to the close alignment of the Bi_2WO_6 CB and the BiOI VB, electrons from the Bi_2WO_6 CB can directly transfer to the BiOI VB, leading to a Z-scheme mechanism. This preserves the more oxidative Bi_2WO_6 valence band holes and the more reductive BiOI conduction band electrons, favoring the generation of more hydroxyl radicals and superoxide radicals, ultimately improving the degradation efficiency [18, 26]. The composite modification can simultaneously leverage the

advantages of Sn doping and BiOI coupling modification, further enhancing photocatalytic activity. The BET results also indicate that the maximum specific surface area is achieved after dual modification, contributing to the enhanced activity. Table 1 summarizes the performance of photocatalysts reported in literatures, showing that the Sn-BiOI/Bi₂WO₆ photocatalyst prepared in the present work exhibits relatively high photocatalytic activity.

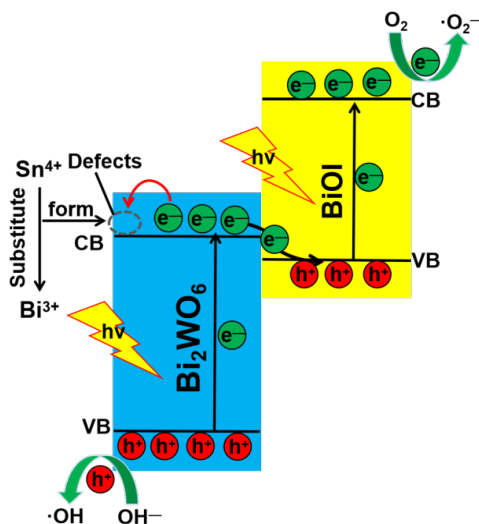


Fig. 11. Schematic diagram of charge transfer for Sn-BiOI/Bi₂WO₆.

Table 1. Literature data on degradation of MB.

Sample	Dosage g·L ⁻¹	Light Source	Degradation degree	First-order reaction rate <i>k</i> (min ⁻¹)	Reference
Bi ₂ WO ₆ /BiOCl	0.5	300 W Xenon lamp	88% (75 min)	0.006	[27]
Bi ₂ WO ₆ /ZnO	0.5	500 W Xenon lamp	98% (120 min)	0.0365	[12]
SnS/Zn ₂ SnO ₄	1	300 W Xenon lamp	95% (60 min)	0.0331	[28]
Bi ₂ WO ₆ /Nb ₂ CTx	0.5	500 W Xenon lam	93% (90 min)	0.0285	[29]
ZnO/ZnFe ₂ O ₄ /TiO ₂	1	300 W Xenon lamp	96% (105 min)	0.0167	[30]
Bi ₂ WO ₆ /WS ₂	0.075	≈850 W/m ² natural solar light	99% (40 min)	0.0482	[31]
TiO ₂ /g-C ₃ N ₄	0.2	300 W Xenon lamp	100% (50 min)	0.097	[32]
Sn-BiOI/Bi ₂ WO ₆	0.25	250 W Xenon lamp	100% (40 min)	0.102	This work

4. Conclusions

The combination of Sn doping and BiOI coupling was used for dual modification of Bi₂WO₆, and the Sn-BiOI/Bi₂WO₆ photocatalytic material was synthesized by hydrothermal route. Characterization results revealed a flower-like structure assembled from nanosheets, with a bandgap width of 2.41 eV, achieving visible light responsiveness. The synergistic effect of Sn doping and BiOI coupling modifications resulted in the increased surface area and enhanced charge separation, leading to superior photodegradation performance compared to single modification. The Sn-BiOI/Bi₂WO₆ exhibited relatively high photocatalytic activity, providing valuable insights for the development of novel photocatalysts.

References

- [1] S. S. Yang, B. H. Ren, S. Y. Chen, S. N. Liu, Y. C. Zhang, Y. Sun. *Dig. J. Nanomater. Bios.* 18, 47-48 (2023); <https://doi.org/10.15251/DJNB.2023.181.47>
- [2] Y. Sun, Y. Gao, J. Y. Zeng, J. Guo, H. Wang. *Mater. Lett.* 279, 128506 (2020); <https://doi.org/10.1016/j.matlet.2020.128506>
- [3] X. D. Zhu, J. Wang, D. X. Yang, J. W. Liu, L. L. He, M. Tang, W. Feng, X. Q. Wu. *RSC. Adv.* 11, 27257 (2021); <https://doi.org/10.1039/d1ra05060ersc.li/rsc-advances>
- [4] H. A. Ahsaine, A. E. Jaouhari, A. Slassi, M. Ezahri, A. Benlhachemi, B. Bakiz, F. Guinneton, J. R. Gavarric. *RSC. Adv.* 6, 101105 (2016); <https://doi.org/10.1039/c6ra22669hwww.rsc.org/advances>
- [5] W. N. Hu, F. Wu, W. Liu. *Chem. Phys.* 552, 111377 (2022); <https://doi.org/10.1016/j.chemphys.2021.111377>
- [6] F. Z. Ren, J. H. Zhang, Y. X. Wang. *RSC. Adv.* 5, 29058 (2015); <https://doi.org/10.1039/c5ra02735g>
- [7] Z. J. Zhang, W. Z. Wang, E. Gao, M. Shang, J. H. Xu. *J. Hazard. Mater.* 196, 255-262 (2011); <https://doi.org/10.1016/j.jhazmat.2011.09.017>
- [8] R. M. Mohamed, E. S. Aazam. *Mater. Res. Bull.* 48, 3572-3578 (2013); <http://dx.doi.org/10.1016/j.materresbull.2013.05.062>
- [9] S. Guo, X. F. Li, H. Q. Wang, F. Dong, Z. B. Wu. *J. Colloid. Interf. Sci.* 369, 373-380 (2012); <http://dx.doi.org/10.1016/j.jcis.2011.12.007>
- [10] Y. L. Zhang, Y. C. Zhao, Z. Xiong, T. Gao, B. G. Gong, P. F. Liu, J. Liu, J. Y. Zhang. *Appl. Catal. B-Environ.* 282, 119534 (2021); <https://doi.org/10.1016/j.apcatb.2020.119534>
- [11] H. D. Gu, L. Yu, J. Wang, M. Ni, T. T. Liu, F. Chen. *Spectrochim. Acta. A.* 177, 58-62 (2017); <http://dx.doi.org/10.1016/j.saa.2017.01.034>
- [12] J. Cheng, Y. Shen, K. Chen, X. Wang, Y. F. Guo, X. J. Zhou, R. B. Bai. *Chinese. J. Catal.* 39, 810-820 (2018); [https://doi.org/10.1016/S1872-2067\(17\)63004-3](https://doi.org/10.1016/S1872-2067(17)63004-3)
- [13] P. P. Teng, Z. A. Li, S. Gao, K. Li, M. Bowkett, N. Copner, Z. H. Liu, X. H. Yang. *Opt. Mater.* 121, 111508 (2021); <https://doi.org/10.1016/j.optmat.2021.111508>
- [14] Z. W. Ni, Y. Shen, L. H. Xu, G. H. Xiang, M. Y. Chen, N. Shen, K. Li, K. Ni. *Appl. Surf. Sci.* 576, 151868 (2022); <https://doi.org/10.1016/j.apsusc.2021.151868>
- [15] W. N. Hu, F. Wu, W. Liu. *Chem. Phys.* 552, 111377 (2022); <https://doi.org/10.1016/j.chemphys.2021.111377>
- [16] J. Wang, X. D. Zhu, F. Q. Qin, Y. X. Wang, Y. Sun, W. Feng. *Mater. Lett.* 314, 131892 (2022); <https://doi.org/10.1016/j.matlet.2022.131892>
- [17] X. D. Zhu, F. Q. Qin, X. P. Zhang, Y. Y. Zhong, J. Wang, Y. Jiao, Y. H. Luo, W. Feng. *Int. J. Mol. Sci.* 23, 8422 (2022); <https://doi.org/10.3390/ijms23158422>
- [18] X. D. Zhu, Y. Y. Zhong, X. P. Zhang, D. X. Yang, L. Zhang, J. Wang, W. Feng, W. M. Zhang. *Arab. J. Chem.* 16, 105286 (2023); <https://doi.org/10.1016/j.arabjc.2023.105286>
- [19] X. T. Gao, S. Zhang, J. C. Liu, S. Q. Xua, Z. H. Li. *RSC. Adv.* 10, 40619 (2020); <https://doi.org/10.1039/d0ra08116g>
- [20] L. Dou, J. J. Li, N. Long, C. X. Lai, J. B. Zhong, J. Z. Li, S. T. Huang. *Surf. Interfaces.* 29, 101787 (2022); <https://doi.org/10.1016/j.surfin.2022.101787>
- [21] A. Etogo, R. Liu, J. B. Ren, L. W. Qi, C. C. Zheng, J. Q. Ning, Y. J. Zhong, Y. Hu. *J. Mater. Chem. A.* 4, 13242-13250 (2016); <https://doi.org/10.1039/C6TA04923K>
- [22] L. Dou, J. B. Zhong, J. Z. Li, R. Pandian, C. Burda. *Appl. Surf. Sci.* 544, 148883 (2021); <https://doi.org/10.1016/j.apsusc.2020.148883>
- [23] N. N. Song, M. H. Zhang, H. Zhou, C. Y. Li, G. Liu, S. Zhong, S. Y. Zhang. *Appl. Surf. Sci.* 495, 143551 (2019); <https://doi.org/10.1016/j.apsusc.2019.143551>
- [24] L. Kan, C. Chang, Q. Wang, X. Y. Wang. *Sep. Purif. Technol.* 297, 121537 (2022); <https://doi.org/10.1016/j.seppur.2022.121537>
- [25] J. Li, J. Shi, Y. B. Li, Z. L. Ding, J. G. Huang. *Ceram. Int.* 47, 8218-8227 (2020); <https://doi.org/10.1016/j.ceramint.2020.11.181>

- [26] G. W. Wang, H. F. Cheng. *Sep. Purif. Technol.* 318, 123949 (2023); <https://doi.org/10.1016/j.seppur.2023.123949>
- [27] H. Y. Jiang, Y. Li, X. Wang, X. D. Hong. *New. J. Chem.* 46, 2627 (2022); <https://doi.org/10.1039/D1NJ05409K>
- [28] Y. J. Wang, F. Xu, L. X. Sun, Y. Y. Li, L. M. Liao, Y. X. Guan, J. H. Lao, Y. K. Yang, T. H. Zhou, Y. Wang, B. Li, K. X. Zhang, Y. J. Zou. *RSC. Adv.* 12, 31985 (2022); <https://doi.org/10.1039/d2ra05519h>
- [29] C. Cui, R. H. Guo, H. Y. Xiao, E. H. Ren, Q. S. Song, C. Xiang, X. X. Lai, J. W. Lan, S. X. Jiang. *Appl. Surf. Sci.* 505, 144595 (2020); <https://doi.org/10.1016/j.apsusc.2019.144595>
- [30] J. J. Zhang, M. Kuang, Y. X. Cao, Z. J. Ji. *Solid. State. Sci.* 129, 106913 (2022); <https://doi.org/10.1016/j.solidstatesciences.2022.106913>
- [31] M. Fiaz, M. Sohail, A. Nafady, G. Will, M. A. Wahab. *Environ. Res.* 234, 116550 (2023); <https://doi.org/10.1016/j.envres.2023.116550>
- [32] B. Lv, X. F. Feng, X. P. Wu, X. M. Wang, X. Zou, H. Z. Wang, F. Q. Zhang. *Diam. Relat. Mater.* 110, 108132 (2020); <https://doi.org/10.1016/j.diamond.2020.108132>